ELSEVIER

Applied Catalysis A: General 164 (1997) 159–169

APPLIED CATALYSIS
A: GENERAL

Effect of altervalent cation-doping on catalytic activity of neodymium sesquioxide for oxidative coupling of methane

Sung Han Lee*, Da Woon Jung, Jung Bae Kim, Yong-Rok Kim*

Department of Chemistry, Yonsei University, Seoul 120-749 and Wonju 220-710, South Korea

Received 21 October 1996; received in revised form 16 April 1997; accepted 21 April 1997

Abstract

Altervalent cation-doped neodymium sesquioxide systems such as Ni/Nd_2O_3, Mn/Nd_2O_3, and Zr/Nd_2O_3 with various doping mole fractions were prepared and the cation-doping effect on the catalytic activity of neodymium oxide in the oxidative coupling of methane was investigated. The catalytic reaction was carried out in a flow reactor system using on-line gas chromatography. The reaction conditions were 550–800°C, feed mole ratio of $CH_4/O_2/He=6/1/5$, total feed flow rate=30.0 $cm^3\ min^{-1}$, and 1 atm of pressure. The present catalysts were effective for the oxidative coupling of methane, the selectivity to higher hydrocarbons was increased by doping the cations into Nd_2O_3. Among the catalysts tested, 5 mol% Zr-doped Nd_2O_3 showed the best C_n-selectivity ($n\geq2$) of 74.1% with a yield of 13.0% at 750°C. Pure Nd_2O_3, Ni-doped Nd_2O_3, and Mn-doped Nd_2O_3 catalysts showed no C_3-hydrocarbon product selectivity, while Zr-doped Nd_2O_3 catalysts showed C_3-hydrocarbon product selectivity ranging from 6% to 12%. When the oxygen-pretreated 5 mol% Ni-doped Nd_2O_3 catalyst was exposed to CH_4 at 400°C, a detectable amount of H_2 was produced, indicating that CH_4 can be selectively activated by oxygen species on the surface. The formation of interstitial oxygen ions through the reaction of oxygen with the oxide is a controlling factor for the catalytic activity of the oxide in the oxidative coupling of methane. The oxygen vacancy formed by doping divalent cation into Nd_2O_3 exerts influence on the formation of active oxygen ion. Zr^{4+}-doping can also increase the concentration of active oxygen ion in the oxide. Defects and active sites in the catalyst are discussed on the basis of solid-state chemistry. © 1997 Elsevier Science B.V.

Keywords: Oxidative coupling of methane; Altervalent cation-doped Nd_2O_3 catalysts

1. Introduction

For the utilization of natural gas (mainly methane), the catalytic conversion of methane to ethylene and ethane has been studied by many investigators since Keller and Bhasin [1] reported the C_2-hydrocarbon production from methane over metal oxide catalysts in 1982. It has been realized that high surface basicity of a catalyst is necessary to enhance the C_2-hydrocarbon selectivity in the oxidative coupling of methane and that alkali promoters can enhance the basicity of the catalyst [2]. According to earlier studies on the oxidative coupling of methane in the presence of metal oxide catalysts, transition metal ions are required in the metal oxide because they are capable of cycling

*Corresponding authors.

PII S0926-860X(97)00166-X

between at least two oxidation states. However, the Li/MgO catalyst which does not contain ions having variable oxidation states or transition metals shows an appreciable catalytic activity in the oxidative coupling of methane [3]. Rare earth metal sesquioxides were also found to be good catalysts for the oxidative coupling of methane, giving high C_2 space–time yields in general [4–7]. Although CeO_2, Pr_6O_{11}, and Tb_4O_7 are unique oxides exhibiting multiple oxidation states among the rare earth metal oxide catalysts, their catalytic activities in the oxidative coupling of methane are very lower than the other oxides such as La_2O_3, Sm_2O_3, and Nd_2O_3. The results indicate that multivalency of metal must not be important in the activation of methane and basic compounds themselves are applicable to the oxidative coupling of methane. Lunsford et al. [7] reported that the catalytic activities of lanthanide oxides in the oxidative coupling of methane are largely enhanced when they are hydrothermally treated, which implies that defects formed in the oxide exert influence on the catalytic activity. Since neodymium sesquioxide is considered to be basic oxide and shows a good C_2-selectivity and a significant CH_4 conversion in the oxidative coupling of methane [8], the promoted neodymium sesquioxide is expected to be a promising catalyst for the oxidative coupling of methane. Neodymium sesquioxide is a p-type semiconductor and its defect structure is easily changed to oxygen vacancy by heating it with hydrogen gas [9,10]. If an altervalent cation is doped into Nd_2O_3, defects such as oxygen vacancy or metal vacancy would be produced in its crystal and such defects may play an important role in the enhancement of catalytic activity in the oxidative coupling of methane. In this work, the lower- and higher-valence cation-doped Nd_2O_3 systems such as Ni/Nd_2O_3, Mn/Nd_2O_3, and Zr/Nd_2O_3 were prepared to investigate the effect of altervalent cation-doping on the catalytic activity of neodymium oxide. We examined their catalytic activities in the oxidative coupling of methane. To characterize the catalysts, X-ray diffractometry (XRD), X-ray photoelectron spectroscopy (XPS), and differential scanning calorimetry (DSC) analyses were performed and electrical conductivity was measured at various oxygen partial pressures at 700°C and 800°C. Defects and active sites in the catalysts are discussed.

2. Experimental

Ni/Nd_2O_3, Mn/Nd_2O_3, and Zr/Nd_2O_3 solid solutions were prepared from high purity nitrates (99.9%, AESAR) $Nd(NO_3)_3 6H_2O$, $Ni(NO_3)_2 6H_2O$, $Mn(NO_3)_2 6H_2O$, and $Zr(NO_3)_4 6H_2O$. Neodymium nitrate and metal nitrate corresponding to the dopant were weighed to give a desired mol% of dopant and mixed together in deionized water at 70°C. The mixture was heated at 120°C with continuous stirring in order to evaporate excess water until a paste remained; this was decomposed under air at 600°C for 6 h, calcined at 1200°C for 96 h in an alumina crucible, and then cooled to room temperature. Pure Nd_2O_3, NiO, and ZrO_2 were obtained by decomposition of the respective metal nitrate. Mn_3O_4 was prepared by heating MnO_2 (99.9%, AESAR) in air at 1000°C and then heating under N_2 at 800°C [11]. To investigate the crystal structure and phase, X-ray powder diffractometry measurements were carried out with a diffractometer (Philips PW 1710) equipped with a curved graphite monochromator in a selected beam path. The surface area of catalyst was determined by the BET method by measuring the adsorption of nitrogen at liquid nitrogen temperature. To get the information about phase changes in the specimens, differential scanning calorimetry (DSC) analysis was performed at a heating rate of 5°C/min in air. The result showed that no phase transitions occur in the present specimens in the temperature range 25–900°C. The O(1s) and C(1s) XPS spectra of the catalysts were obtained using VG ESCALAB with a high-pressure cell attached to the analytical vacuum chamber. The powdered samples were made into pellets, mounted on a transferable sample holder, and then the O(1s) and C(1s) binding energies were obtained for the catalysts after calcination at 600°C and after treatment in the reactant mixture($CH_4/O_2/He$) at 600°C in the high-pressure cell. Electrical conductivity was measured as a function of P_{O_2} in the range 10^{-5}–10^{-1} atm at 700°C and 800°C by means of the four-contact method. To measure the electrical conductivity, the powdered samples were made into pellets under a pressure of 100 MPa under vacuum. The pellets were sintered in dry air at 1200°C for 96 h, annealed at 1000°C for 48 h, and then quenched to room temperature.

Kinetic studies using an on-line gas chromatography system were carried out in a conventional singlepass fixed-bed type flow reactor operated at 1 atm. The reactor was made of alumina tubing with 1.2 cm diameter and 30 cm length. The powdered catalyst was held between alumina wool plugs in the middle of the reactor. The section beyond the catalyst bed in the reactor was filled with alumina beads to reduce the free space, and the reactor was kept in a vertical tubular furnace. A K-type thermocouple sealed with an alumina tube was placed just above the catalysts in the reactor to control the reaction temperature. The purity of gaseous oxygen, methane, and helium was greater than 99.99%; the reaction gases were purified by passing over a bed of molecular sieve to remove water before introducing them into the reactor. Before each activity measurement, the catalyst was calcined in situ at 500°C in a flow of O_2 (10 ml min^{-1}) for 1 h, the reaction gases were co-fed to the reactor, and then the reactor temperature ramped to the reaction temperature. Gas analysis was performed by on-line gas chromatography using a thermal conductivity detector and a flame ionization detector. Each blank test was performed over inert alumina beads in the absence of catalyst and approximately 2–4% conversion of methane to CO_2 was obtained in the reaction temperature range 550–800°C. The major products were CO, CO_2, H_2O, C_2H_4, C_2H_6, C_3H_6, and C_3H_8. Water was removed from the products by a trap placed at the reactor exit. Gas compositions were calculated using external standard gas mixtures. The conversion of methane was calculated from the amounts of products generated and the methane introduced in the feed stream. The selectivities were calculated on the basis of the conversion of methane to each product and the yield was obtained from the CH_4 conversion and selectivity to each product. The closures on the carbon material balances were within 4%. The following conditions were used to compare the activity of the catalysts: atmospheric pressure, a 0.5 g sample loading of catalyst, a feed mole ratio of $CH_4/O_2/He=6/1/5$, and a feed flow rate at ambient conditions of 30.0 cm^{3}min^{-1}. The conversion of reactants and selectivities to products were typically compared after 2 h time-on-stream. The reaction of CH_4 with O_2-pretreated catalyst and CO-pretreated catalyst, catalyst (2.0 g) was loaded into the flow reactor, heated in situ at 600°C in a flow of He for 0.5 h, then oxidized at 400°C in a flow of dry O_2 (10 ml min^{-1}) for 1 h or reduced at 400°C in a flow of dry CO for 0.5 h. The reactor was cooled to room temperature, then helium gas was passed to remove any O_2 or CO gas remaining in the reactor. The reactor temperature was ramped to 400°C using a programmable temperature controller and then the mixture of CH_4 and He was fed to the flow reactor with various flow rates. The products were analyzed immediately after introduction of the mixture into the reactor, using on-line gas chromatography.

3. Results and discussion

To investigate the crystal structure, the formation of solid solution, and the precision lattice parameters, the X-ray powder diffraction anaysis was performed for each sintered catalyst. The determination of precision lattice parameters was made using Nelson–Riley function. Pure Nd_2O_3 prepared by decomposition of $Nd(NO_3)_26H_2O$ showed only the presence of Nd_2O_3 crystalline phase with a hexagonal structure, the lattice parameters obtained were a=3.834 and c=6.005 Å, which agree with the values (a=3.831 and c=5.999 Å) listed in ASTM. Lattice parameters of the altervalent cation-doped Nd_2O_3 catalysts were also obtained for the single-phase hexagonal structure, the values are listed in Table 1. Strickler and Calson [12] reported that the lattice parameters show linearity only in the

Table 1
Lattice parameters and BET surface areas of pure and doped Nd_2O_3 catalysts

Sample	Lattice parameter		BET surface area (m^2/g)
	a (Å)	b (Å)	
Pure Nd_2O_3	3.834	6.005	12.7
5 mol% Ni/Nd_2O_3	3.821	5.941	35.2
8 mol% Mn/Nd_2O_3	3.825	5.991	26.1
5 mol% Zr/Nd_2O_3	3.823	5.977	27.4

region where complete solid solutions are established in the plots of lattice parameters vs. dopant mol% for various cation-doped solid solutions. Thus, the formation of solid solutions can be interpreted from the linearity of the data points for each sample in the plot of lattice parameters vs. dopant mol%. The plots of lattice parameters vs. dopant mol% showed good linearities up to the doping level of 10 mol% Ni for Ni/Nd_2O_3, 12 mol% Mn for Mn/Nd_2O_3, and 10 mol% Zr for Zr/Nd_2O_3 system. However, small amounts of NiO, Mn_3O_4, and ZrO_2 phases unreacted in the oxide were observed from the X-ray diffraction patterns of 10 mol% Ni/Nd_2O_3, 12 mol% Mn/Nd_2O_3, and 10 mol% Zr/Nd_2O_3 system, respectively. Applying Vegard's law to the present catalysts formed by random substitution or distribution of ions, one assumes implicitly that the changes in lattice parameters with composition are governed by the relative sizes of the atoms or ions which are active in the solid-solution process in a simple substitutional mechanism. The decrease in lattice parameters for the hexagonal phase of the altervalent cation-doped Nd_2O_3 catalysts shown in Table 1 can be explained by the fact that the ionic radii of Ni^{2+}(0.72 Å), Mn^{2+}(0.80 Å), and Zr^{4+}(0.80 Å) are smaller than that of Nd^{3+}(1.08 Å), or, in other words, that the lattice parameters decrease because of the increasing addition of dopant with smaller ionic radius. The linear decrease in the lattice parameters for the hexagonal phase of the cation-doped Nd_2O_3 is in agreement with Vegard's law expected for a true solid solution. Fig. 1 shows the O(1s) XPS spectra of pure Nd_2O_3 and 5 mol% Ni-doped Nd_2O_3. The O(1s) XPS spectra of Nd_2O_3 after calcination at 600°C in Fig. 1(A) present a maximum at 530.5 eV and a large shoulder at 533.0 eV. Fig. 1(B) and (C) are the O(1s) spectra of 5 mol% Ni-doped Nd_2O_3 after calcination and after treatment in the reactant mixture at 600°C, respectively; in these figures large peaks are observed at 529.6 eV and shoulder peaks are observed around 532.3 eV. In case of rare earth metal oxide, the O(1s) binding energy arising from hydroxyl or carbonate ions is higher than that arising from lattice oxygens in general. Since hydroxyl and carbonate ions are close in their O(1s) binding energies, the higher binding energies in Fig. 1 are believed to be a combination of peaks corresponding to hydroxyl and carbonate ions. We also investigated the C(1s) binding energies of 5 mol% Ni-doped

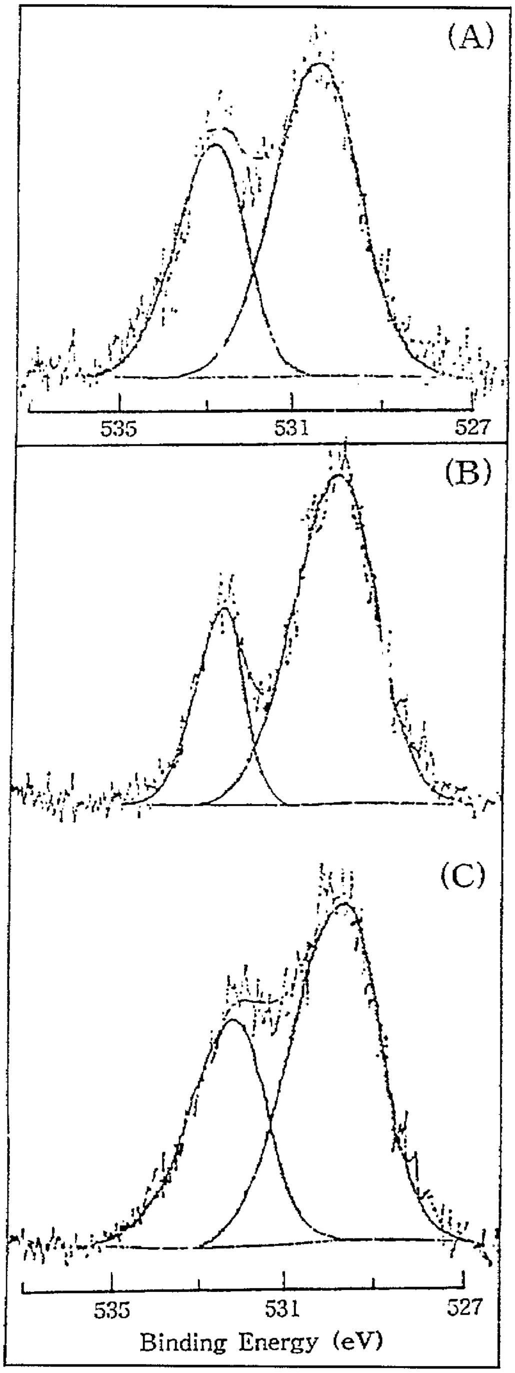

Fig. 1. O(1s) XPS spectra: (A) Pure Nd_2O_3 and (B) 5.0 mol% Ni-doped Nd_2O_3; (C) 5.0 mol% Ni-doped Nd_2O_3 after treatment in the reactant mixture ($CH_4/O_2/He$) at 600°C.

Nd_2O_3 after calcination and after treatment in the reactant mixture at 600°C, respectively, in which two peaks were observed at 284.6 and 289.1 eV. The intensity of C(1s) peak at 289.1 eV, corresponding typically to a carbon belonging to a carbonate ion, was significantly diminished after treatment in the reactant mixture at 600°C, which implies the desorption of CO_2 from the surface or the decomposition of carbonate phase through the reaction. According to the TPD analysis of Nd_2O_3 exposed to air, carbon dioxide is evolved from the surface around 500°C [13]. Therefore, it is believed that the O(1s) peak observed at 532.3 eV in Fig. 1(C) is largely due to hydroxyl ions formed on the surface. We measured the electrical conductivities of the present specimens at various P_{O_2}'s at 700 and 800°C. As presented in Table 2, the electrical conductivities of pure Nd_2O_3, 5 mol% Ni-doped Nd_2O_3, and 5 mol% Zr-doped Nd_2O_3 were increased with increasing temperature and oxygen partial pressure, indicating the specimens to be p-type semiconductors. The electrical conductivity of Ni-doped Nd_2O_3 increased with increasing the Ni mol%, while that of Zr-doped Nd_2O_3 decreased with increasing the Zr mol%. In this work, pure Nd_2O_3, Ni-, Mn-, and Zr-doped Nd_2O_3 catalysts revealed appreciable catalytic activities in the oxidative coupling of methane. In Table 3, the C_2-selectivity of pure Nd_2O_3, 56.9%, is rather appreciable, but the catalytic activities of pure NiO and Mn_3O_4 are negligible. The C_n-selectivity of Nd_2O_3 ($n \geq 2$) was enhanced by the dopants. Among the catalysts tested in this work, the 5 mol% Zr-doped Nd_2O_3 catalyst showed the best C_n-selectivity of 74.1% at 750°C. Table 4 shows the methane conversion and product selectivity of Ni/Nd_2O_3, Mn/

Table 2
Electrical conductivities of pure, Ni-, and Zr-doped Nd_2O_3 at various P_{O_2}'s at 700°C and 800°C

Sample	Temp. (°C)	Log conductivity (Ω^{-1} cm^{-1})		
		P_{O_2}		
		1.0×10^{-1}	1.0×10^{-3}	1.0×10^{-5}
Nd_2O_3	700	−4.15	−4.53	−5.01
	800	−3.80	−4.36	−4.95
1 mol% Ni/Nd_2O_3	700	−3.85	—	—
2 mol% Ni/Nd_2O_3	700	−3.45	—	—
5 mol% Ni/Nd_2O_3	700	−3.32	−3.64	−3.98
	800	−3.06	−3.52	−3.95
1 mol% Zr/Nd_2O_3	700	−4.41	—	—
3 mol% Zr/Nd_2O_3	700	−4.50	—	—
5 mol% Zr/Nd_2O_3	700	−4.61	−5.26	−5.95
	800	−4.00	−4.68	−5.37

Table 3
Methane conversion and product selectivity for oxidative coupling of methane over various metal oxide catalysts

Catalyst	Temp.	Methane	Selectivity (%)					
	(°C)	conversion (%)	CO	CO_2	C_2H_4	C_2H_6	C_3^+	C_n total
NiO	700	20.3	99.0	1.0	0	0	0	0
ZrO_2	775	8.9	35.5	29.0	4.5	31.0	0	35.5
Mn_3O_4	750	15.1	3.1	88.1	0	8.7	0	8.7
Nd_2O_3	750	16.1	0	43.1	38.2	18.7	0	56.9
5% Ni/Nd_2O_3 [a]	650	16.4	0	30.7	37.8	31.6	0	69.4
8% Mn/Nd_2O_3 [a]	720	17.3	0.6	30.4	35.0	34.0	0	69.0
5% Zr/Nd_2O_3 [a]	750	17.5	0	25.9	28.9	37.3	7.9	74.1

[a] Atomic mol%, catalyst weight=0.5 g; total pressure=1 atm; feed mole ratio of $CH_4/O_2/He$=6/1/5; total feed flow rate=30.0 cm^3 min^{-1}.

Table 4
Catalytic activity and selectivity for oxidative coupling of methane over altervalent cation-incorporated Nd_2O_3 catalysts

Catalyst[a]	Temp.	Methane	Selectivity (%)					
	(°C)	conversion (%)	CO	CO_2	C_2H_4	C_2H_6	C_3^+	C_n total
1% Ni/Nd_2O_3	650	15.8	0	46.0	30.8	23.2	0	54.0
2% Ni/Nd_2O_3	650	16.0	0	36.5	34.8	28.7	0	63.5
5% Ni/Nd_2O_3	650	16.4	0	30.7	37.8	31.6	0	69.4
10% Ni/Nd_2O_3	650	15.7	0	46.6	27.3	26.1	0	53.4
2% Mn/Nd_2O_3	720	15.3	3.7	37.8	30.5	28.0	0	58.5
5% Mn/Nd_2O_3	720	18.5	1.4	38.8	30.4	29.4	0	59.8
8% Mn/Nd_2O_3	720	17.3	0.6	30.4	35.0	34.0	0	69.0
10% Mn/Nd_2O_3	720	17.1	2.2	37.7	32.1	28.0	0	60.1
12% Mn/Nd_2O_3	720	14.2	5.8	58.3	20.5	15.4	0	35.9
1% Zr/Nd_2O_3	750	16.4	0	31.0	25.0	32.0	12.0	69.0
3% Zr/Nd_2O_3	750	17.0	0	28.7	28.0	34.3	9.0	71.3
5% Zr/Nd_2O_3	750	17.5	0	25.9	28.9	37.3	7.9	74.1
8% Zr/Nd_2O_3	750	17.4	0	27.5	25.3	40.1	7.1	72.5
10% Zr/Nd_2O_3	750	17.1	0	27.6	25.0	41.1	6.3	72.4

[a]Atomic mol%, catalyst weight=0.5 g; total pressure=1 atm; feed mole ratio of $CH_4/O_2/He=6/1/5$; total feed flow rate=30.0 $cm^3\ min^{-1}$.

Nd_2O_3, and Zr/Nd_2O_3 catalysts with various mole fractions. The C_n-selectivity maxima were observed at the doping level of 5 mol% Ni for Ni/Nd_2O_3, 8 mol% Mn for Mn/Nd_2O_3, and 5 mol% Zr for Zr/Nd_2O_3 system. It is interesting to note that a significant amount of C_3 hydrocarbons such as propene and propane was produced on Zr-doped Nd_2O_3 catalyst, but was not observed on Nd_2O_3, Ni/Nd_2O_3, and Mn/Nd_2O_3 catalysts. Fig. 2 shows variations of methane conversion and product selectivity with temperature over 5 mol% Zr/Nd_2O_3 catalyst. The C_n-selectivity maxima were observed around 650°C for 5 mol% Ni/Nd_2O_3, 720°C for 8 mol% Mn/Nd_2O_3, and 750°C for 5 mol% Zr/Nd_2O_3. The ratio of ethylene/ethane is increased with increasing temperature for the present catalysts.

Many investigators have reported on the nature of active sites in metal oxide catalyst for the oxidative coupling of methane. Although there is considerable evidence that peroxide ions(O_2^{2-}) play a role in the activation of methane over certain catalyst [14], it is generally accepted that the O^- species on the surface of metal oxide catalyst selectively activate methane. Morikawa et al. [4] studied the oxidative coupling of methane over rare earth metal oxide catalysts and suggested that O^- ions produced on oxygen vacancy sites or basic sites may abstract hydrogen from methane, forming methyl radicals, and deep oxidation of CH_4 may be caused by surface O^{2-} or by the diatomic oxygen adsorbed. According to the isotope transient kinetic study on the oxidative coupling of methane by Mirodatos et al. [15], the surface residence time of activated species on lanthana catalyst is below the time resolution of 1 ms, characteristic of the temporal analysis of product reactor (TAP), which makes it difficult to detect the O^- species on lanthana. They proposed from the TAP experiment that the electrophilic site formed during O_2 adsorption is O^- or O_2^- and both species are very likely to be in equilibrium since they result from a series of equilibrated steps where oxygen is progressively enriched in electrons. Onishi et al. [16] studied the O_2 adsorption on H_2-reduced cerium oxide using in situ FT–IR spectroscopy and found that superoxide species (O_2^-) are formed immediately after introduction of gaseous oxygen, successively converted into O_2^{2-}, O^-, and finally into O^{2-}(latt). Superoxide (O_2^-) and peroxide (O_2^{2-}) species can be considered as the intermediates formed during oxygen dissociation, and their existence mainly depends on the basicity of metal oxide and the existence of suitable sites for the stability of the formed species. It was also proposed that the formation of O^- becomes more probable when the temperature is increased [17,18].

In the present work, the catalytic activity was increased with the altervalent cation substitution for

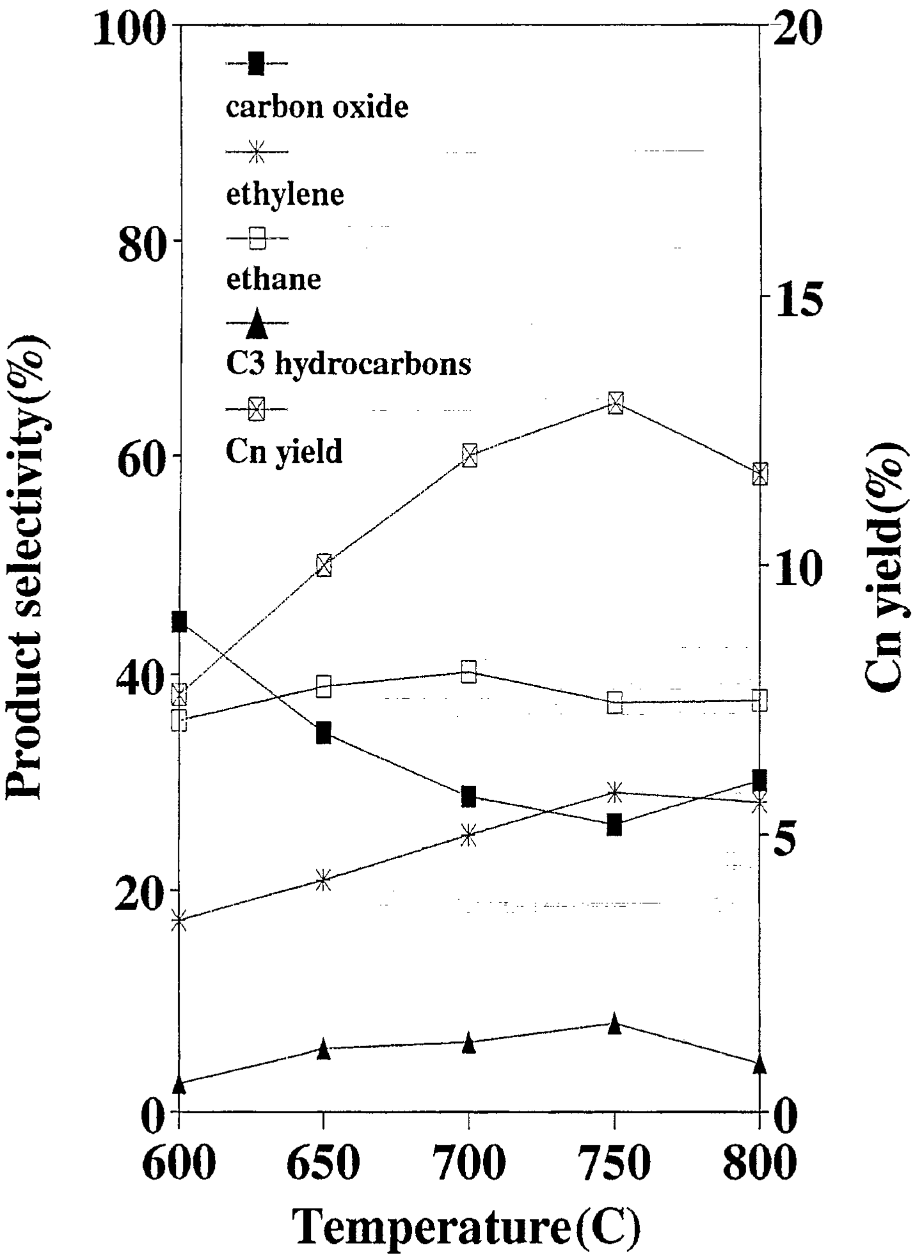

Fig. 2. Variations of methane conversion and product selectivity with temperature for 5 mol% Zr-doped Nd_2O_3 catalyst.

Nd of Nd_2O_3, which shows that defects formed in the oxide catalyst act as an important factor controlling the catalytic activity. In Fig. 1, the O(1s) binding energy at 530.5 eV corresponding to lattice oxygen was shifted to 529.6 eV when Ni^{2+} cation was doped into Nd_2O_3. Since the electron pair donating ability of a metal oxide is assumed to be expressed by the O(1s) binding energy, the O(1s) binding energy arising from lattice oxygen is a measure of the basic strength of metal oxide. Such basic strength generally increases

Table 5
Quantity of H_2 produced from methane over O_2-preadsorbed 5 mol% Ni-doped Nd_2O_3 catalyst

Contact time[a] (g min/ml)	Quantity of H_2 formation (mol/g)
0.05	1.8×10^{-6}
0.10	2.2×10^{-6}
0.20	3.1×10^{-6}
0.40	3.2×10^{-6}

Reaction temperature: 400°C.
[a]Weight of catalyst/volumetric flow rate.

with decreasing the O(1s) binding energy [19]. Therefore, the chemical shift in the O(1s) binding energy means that the basicity of Nd_2O_3 is increased by Ni^{2+}-doping. Namely, when the divalent cation is doped into Nd_2O_3, an electron donor center such as oxygen vacancy can be created in the oxide, which can lead to the improvement of catalytic activity in the oxidative coupling of methane. We investigated the reactivity of CH_4 with the surface of O_2-pretreated and CO-pretreated catalysts at 400°C, in which an evolution of H_2 gas was observed. Hydrogen gas was observed as a trace on the O_2-pretreated Nd_2O_3 and the CO-pretreated 5 mol% Ni-doped Nd_2O_3, while a detectable amount of H_2 was produced on the O_2-pretreated 5 mol% Ni-doped Nd_2O_3 as given in Table 5. The result indicates that oxygen species on the surface activate CH_4, since H_2 molecules are produced via the abstraction of hydrogen from CH_4, although the nature of active oxygen species remains to be determined. In Table 2, the electrical conductivities of the Ni-doped Nd_2O_3 increase with increasing P_{O_2}. If a divalent cation such as Ni^{2+} or Mn^{2+} is heavily doped into neodymium sesquioxide, oxygen vacancies would be generated as charge-compensating defects and the reaction can be represented as

$$MO \rightleftharpoons M'_{Nd} + O_o{}^x + 1/2V\ddot{o} \tag{1}$$

where $M_{Nd}{}'$ is an effectively singly ionized divalent-cation doped into a Nd site and the divalent cation acts as an electron hole donor. As presented in the previous paper [21], we studied the CO oxidation over perovskite-type metal oxide catalyst using CO_2-laser-based photoacoustic spectroscopy and showed that oxygen vacancies formed in the catalyst are adsorption sites for oxygen molecules. According to a study on the oxidative coupling of methane over metal oxide catalyst using the high resolution electron energy loss spectroscopy (HREELS) by Goodman et al. [22], an oxygen vacancy with two trapped electrons in doped metal oxide can act as the active centers in the reaction, such a result is conformable with ours. If O_2 is adsorbed on an oxygen vacancy defect ($V\ddot{o}$-$2e^-$), the reaction can be represented as the following equilibrium:

$$O_2(g) + 2e^- \rightleftharpoons 2O^-(ads)(\text{or } O_2^{2-}(ads)) \tag{2}$$

where e^- is a conduction electron trapped at an oxygen vacancy. Since the chemisorption of O_2 on oxygen vacancy dissipates the conduction electron in the oxide, the electrical conductivity should decrease with increasing P_{O_2}, which is not consistent with the result in Table 2. Therefore, we have to consider another process for the generation of a p-type charge carrier such as an electron hole at temperatures above 700°C. If oxygens are further moved to interstitial positions in the oxide, an electron hole would be generated and the process can be represented as the following equilibrium:

$$1/2O_2 \rightleftharpoons O_i{}^x \tag{3}$$

where $O_i{}^x$ indicates a neutral interstitial oxygen. The neutral interstitial oxygen atoms may in principle be ionized to yield electron holes and oxygen ions with negative effective charges and the processes may be written as

$$O_i{}^x \rightleftharpoons O'_i + h^{\bullet} \tag{4}$$

$$O_i{}' \rightleftharpoons O_i{}'' + h^{\bullet} \tag{5}$$

According to the report of Berard et al. [23], the activation energy for the diffusion of a cation in lanthanide oxide is larger than that of an anion and the movement of oxygen ions through the ⟨1 1 1⟩ open pathway is promoted. Eyring et al. [24] also reported that the movement of oxygen in lanthanide oxides is possible even at the low temperature of 400°C, but no mobile cations are observed even at the high temperature of 1200°C. Based on these reports, it is suggested that the diffusion of oxygen in the divalent cation-doped Nd_2O_3 systems such as Ni^{2+}/Nd_2O_3 and Mn^{2+}/Nd_2O_3 is promoted because the oxides are expected to contain oxygen vacancies in them. When the oxygen diffusion according to equilibrium (3) becomes predominant, the concentrations of electron holes and interstitial oxygen ions are simultaneously increased, which leads to a p-type conductivity of the oxide, as shown in Table 2.

In case of oxygen interstitial model, the oxygen partial pressure dependence of the conductivity can be derived from the equilibrium between interstitial oxygen ions and gaseous oxygen. When p=2 $[O_i'']\gg[V\ddot{o}]$, that is, for large excess of oxygen, the electrical conductivity is proportional to $Po_2^{1/6}$ and when $[O_i'']\simeq[V\ddot{o}]$, the electrical conductivity is proportional to $Po_2^{1/4}$ [25]. Since the amount of excess oxygen in Nd_2O_3 decreases with increasing temperature and oxygen vacancies are produced in the oxide at high temperatures above 800°C [9], electron holes can be generated from the interaction between oxygen molecules and oxygen vacancies and then the oxygen partial pressure dependence of the conductivity can be varied with temperature. Electrical conductivities of 5 mol% Ni-doped Nd_2O_3 measured at 700°C in Table 2 are fitted to $\sigma \propto Po_2^{1/6}$, indicating that the electrical conduction is carried by the electron–hole generated by ionization of interstitial oxygen. Assuming random diffusion, a relation between conductivity and diffusion coefficient is given by

$$\sigma = cz^2e^2D/kT, \tag{6}$$

where σ is the electrical conductivity, z the valence, and c the concentration of the particle [20]. Stone et al. studied oxygen diffusion in the temperature range 700–1000°C by using the O^{18} exchange technique and found the diffusion coefficient in Nd_2O_3 to be $D=1.3\times10^{-4}\exp(-31\ \text{kcal mol}^{-1}/RT)$ [26]. We estimated concentrations of interstitial oxygen in Ni-doped Nd_2O_3 catalysts at 700°C from the conductivity data in Table 2 and the diffusion coefficient in Nd_2O_3 by Eq. (6). Fig. 3 shows variations of C_2-selectivity and C_2 yield with the concentration of interstitial oxygen in Ni-doped Nd_2O_3 system at 700°C, in which the C_2-selectivity and C_2 yield increase with increasing the concentration of interstitial oxygen. Since the singly charged interstitial oxygen ion, being likely to be in equilibrium with the doubly charged interstitial oxygen ion as represented by equilibrium (5), holds the same negative charge with O^-(ads), it is believed that the O_i' ions existing near the surface can activate methane as O^-(ads) ions and thus the catalytic activity of the oxide in the oxidative coupling of methane can be enhanced as shown in Fig. 3.

On the other hand, when ZrO_2 is dissolved into $NdO_{1.5+x}$, ZrO_2 can react with cation vacancies as follows:

$$ZrO_2 + V_{Nd}''' \rightleftharpoons Zr_{Nd}^{\bullet} + 2O_i'' \tag{7}$$

where $Zr_{Nd}^{\bullet}$ is singly positively charged Zr atom in Nd lattice site. As the amount of ZrO_2 doped in the oxide increases, some interstitial oxygens being thermodynamically unstable can be introduced to lattice sites

$$3O_i'' \rightleftharpoons 3O_o + 2V_{Nd}''' \tag{8}$$

If Nd_2O_3 is metal deficient and predominantly contains charged metal vacancies (V_{Nd}'''), the dissolution of ZrO_2 would simultaneously increase the concentration of metal vacancies and electron holes; then a p-type conductivity of the oxide can be observed. As shown in Table 2, the electrical conductivities measured at 1.0×10^{-1} atm of P_{O_2} decrease as the Zr mol% increases, which implies that the equilibrium (8) moves toward the left-hand side, i.e., the movement of lattice oxygen to an interstitial position in the oxide. Bratton [27] measured X-ray and pycnometric densities of Zr-doped Y_2O_3 systems. The system is similar to Zr-doped Nd_2O_3 in structure. He demonstrated that defects in the oxide are interstitial oxygens, supporting the conclusion that interstitial oxygens are predominant defects in the Zr-doped Nd_2O_3. As mentioned above, since the O_i' and O_i'' ions are likely to be in equilibrium and the O_i' ions near the surface can act as active sites for methane molecules, methane can be selectively activated on the Zr-doped Nd_2O_3 catalyst, resulting in the enhancement of catalytic activity in the oxidative coupling of methane. In this work, Zr-doped Nd_2O_3 catalysts showed a C_3-selectivity, while pure Nd_2O_3, Ni- and Mn-doped Nd_2O_3 catalysts did not show any C_3-selectivity, as given in Table 4. The result enables us to consider that there is a relation between the mobility of oxygen ion and the C_n-selectivity of the metal oxide catalyst in the oxidative coupling of methane.

In the case of the pure Nd_2O_3 catalyst, its electrical conductivities measured at 700°C and 800°C increased with increasing P_{O_2}, as shown in Table 2, indicating a p-type character. It has been reported that neodymium sesquioxide shows an oxygen uptake in air above 400°C; the amount of oxygen uptake, i.e., excess oxygen, is expressed as x in $NdO_{1.5+x}$, it ranged from 1.8×10^{-4} at 400°C to 0.6×10^{-4} at 800°C. Thus

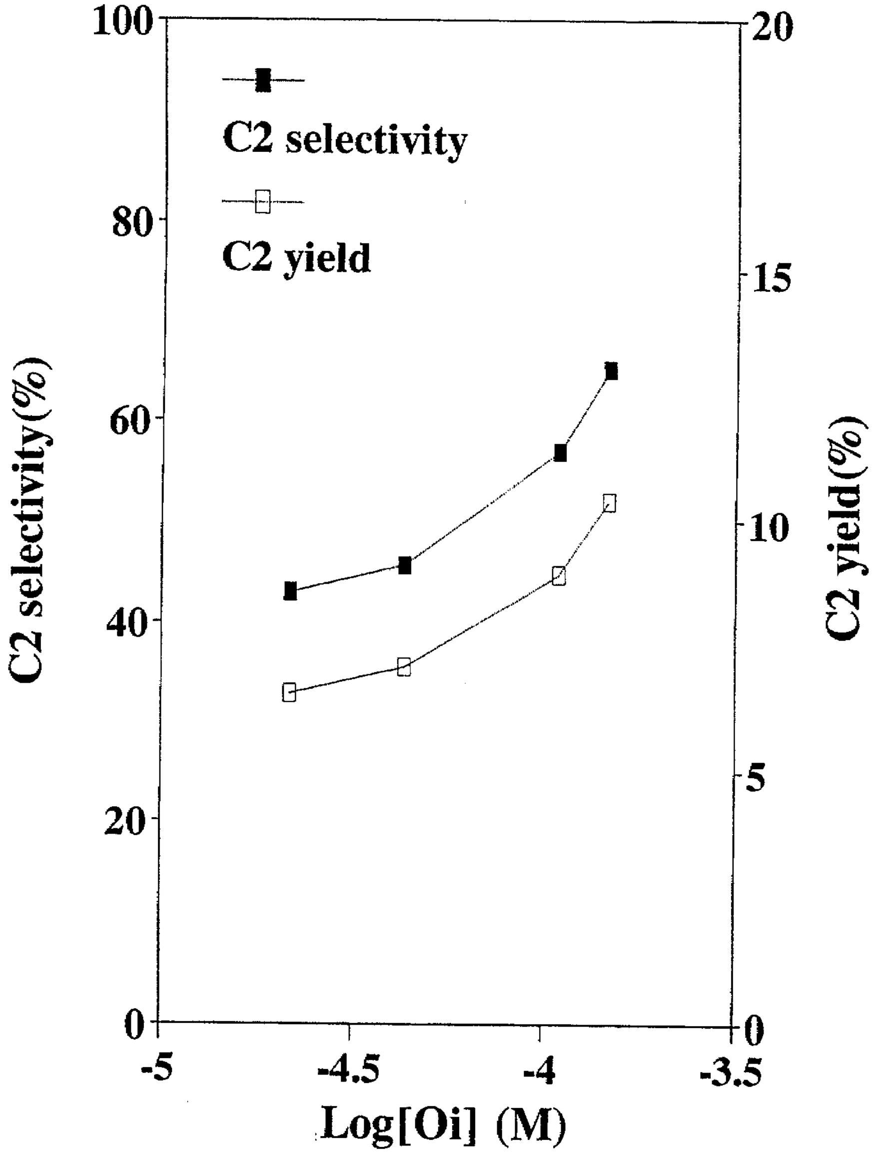

Fig. 3. Variations of C_2 selectivity and C_2 yield with concentration of interstitial oxygen at 700°C for Ni-doped Nd_2O_3 catalysts.

the O_2-chemisorption is reversible and rapid above 400°C, suggesting fast oxygen diffusion in the oxide [9,20]. The predominant defects in excess-oxygen metal oxide such as Nd_2O_3 may be metal vacancies or interstitial oxygen atoms. When neutral interstitial oxygens are produced through the reaction of oxygen with Nd_2O_3 according to equilibrium (3) and the neutral interstitial oxygen atoms are ionized to yield electron holes and oxygen ions with negative effective charges, the oxide will show a p-type conductivity and a catalytic activity in the activation of methane, as obtained in this work. Considering the appreciable catalytic activity of Nd_2O_3, the oxygen diffusion according to equilibrium (3) is believed to be predominant rather than the formation of metal vacancy at the reaction temperatures. In conclusion, the interstitial oxygen ions resulting from oxygen diffusion as well as the O^{-}(ads) species chemisorbed on oxygen vacancy act as active sites for methane in the oxidative coupling of methane and the mobility of oxygen ion in the catalyst seems to exert influence on the selectivity to higher hydrocarbons.

Acknowledgements

This work was supported by grant from the Korea Science and Engineering Foundation(KOSEF 951-0302-022-2).

References

[1] G.E. Keller, M.M. Bhasin, J. Catal. 73 (1982) 9.
[2] Y. Feng, J. Nirranen, D. Gutman, J. Phys. Chem. 95 (1991) 6558.
[3] T. Ito, J.X. Wang, C.H. Lin, J.H. Lunsford, J. Am. Chem. Soc. 107 (1985) 5062.
[4] K. Otsuka, K. Jinno, A. Morikawa, J. Catal. 100 (1986) 353.
[5] S. Lacombe, C. Geantet, C. Mirodatos, J. Catal. 151 (1994) 439.
[6] V.R. Choudhary, V.H. Rane, J. Chem. Soc. Faraday Trans. 90 (1994) 3357.
[7] K.D. Campbell, H. Zhang, J.H. Lunsford, J. Phys. Chem. 92 (1988) 750.
[8] M.P. Rosynek, Catal. Rev. Sci. Eng. 16 (1977) 111.
[9] M.F. Barrett, T.I. Barry, J. Inorg. Nucl. Chem. 27 (1965) 1483.
[10] V. Pratap, B.K. Verma, H.B. Lal, Proc. Natl. Acad. Sci., India Sect. A48 (1978) 20.
[11] R. Burch, S. Chalker, G.D. Squire, S.C. Tsang, J. Chem. Soc. Faraday Trans. 86(9) (1990) 1607.
[12] D.W. Strickler, W.G. Carlson, J. Am. Ceram. Soc. 47 (1964) 122.
[13] S. Bernal, F.J. Botana, R. Garcia, J.M. Rodriguez-izquierdo, Reactivity of Solids 4 (1987) 23.
[14] J.H. Lunsford, Angew. Chem. Int. Ed. Engl. 34 (1995) 970.
[15] S. Lacombe, H. Zanthoff, C. Mirodatos, J. Catal. 155 (1995) 106.
[16] C. Li, K. Domen, K. Maruya, T. Onishi, J. Am. Chem. Soc. 111 (1989) 7683.
[17] G.U. Kulkarni, C.N.R. Rao, M.W. Roberts, J. Phys. Chem. 99 (1995) 3310.
[18] T. Yang, L. Feng, S. Shen, J. Catal. 145 (1994) 384.
[19] K. Tanabe, in: J.R. Anderson, M. Boudart (Eds.), Catalysis: Science and Technology, vol. 2, Springer, New York, 1981, p. 231.
[20] P. Kofstad, Nonstoichiometry, Diffusion, and Electrical Conductivity in Binary Metal Oxides, Wiley-Interscience, New York, 1972, p. 265.
[21] H.J. Jung, J.T. Lim, S.H. Lee, Y.R. Kim, J.G. Choi, J. Phys. Chem. 100 (1996) 10243.
[22] M.-C. Wu, C.H. Truong, K. Coulter, D.W. Goodman, J. Catal. 140 (1993) 344.
[23] M.F. Berard, D.R. Wilder, J. Am. Cer. Soc. 52 (1969) 85.
[24] L. Eyring, B. Holmberg, Nonstoichiometric compounds, Am. Chem. Soc., Washington DC, 1963, p. 46.
[25] O.T. Sorensen, Nonstoichiometric oxides, Academic Press, New York, 1981, p. 283.
[26] G.D. Stone, G.R. Weber, L. Eyring, Mass transport in oxides, National Bureau of Standards Special Publication 296, Washington DC, 1968, p. 179.
[27] R.J. Bratton, J. Am. Cer. Soc. 52 (1969) 213.